Supporting information

Magnetic structure and internal field nuclear magnetic resonance in cobalt nanowires

Pascal Scholzen,[1] Guillaume Lang,[2] Andrey S. Andreev,[3] Alberto Quintana,[4] James Malloy,[4] Christopher J. Jensen,[4] Kai Liu,[4] and Jean-Baptiste d'Espinose de Lacaillerie[1]**

(1) SIMM, ESPCI Paris, Université PSL, CNRS UMR 7615, 10 Rue Vauquelin, 75005, Paris, France.

(2) LPEM, ESPCI Paris, Université PSL, CNRS UMR 8213, 10 Rue Vauquelin, 75005, Paris, France.

(3) TotalEnergies One Tech Belgium (TEOTB), Zone Industrielle C, 7181 Feluy, Belgium

(4) Physics Department, Georgetown University, Washington, DC 20057, USA

KEYWORDS. ^{59}Co NMR, internal field NMR, ferromagnetism, metallic nanostructures, nanomagnetism, FNR.

Scherrer analysis for particle size and lattice parameters

In order to perform the Scherrer analysis, the different peaks of the diffractograms in Figure 3 were fitted with a Pseudo-Voigt line shape and considering the $K_{\alpha,1}$ and $K_{\alpha,2}$ contributions. The size (D) of the crystallites is then determined using Scherrer's formula:[1]

$$D = \frac{K\lambda}{\beta\, cos\theta}$$

with K the form/Scherrer factor (set equal to 0.9, because unknown crystallite shape), λ the wavelength (Cu anode => 0.15406 nm), β the FWHM of the Pseudo-Voigt peak (2θ in rad, after subtraction of the machine contribution: 0.08°) and θ the Bragg angle (in rad).

Table S1. Crystallite size estimates obtained from the XRD diffraction peaks for the different samples analyzed in this work.

		200 nm with additives		200 nm no additives	
Angle 2θ (°)	Diffraction planes	FWHM (°)	Crystallite size (nm)	FWHM (°)	Crystallite size (nm)
41.6	*hcp* (100)	/	/	0.44	23.6
44.3	*hcp* (002)/ *fcc* (111)	1.05	8.8	0.91	10.3
51.5	*fcc* (200)	1.9	4.8	/	
75.9	*hcp* (110)/ *fcc* (220)	1.5	7.1	0.66	17.2
92.4	*hcp* (112)/ *fcc* (311)	1.6	7.5	1.2	10.2

The lattice parameters of the cubic fcc phase in the 200 nm samples can be calculated using the formula:

$$\frac{1}{d^2} = \frac{h^2 + l^2 + k^2}{a^2}$$

With d^2 the interplanar spacing of and h, l, k the Miller indices of the diffraction plane and a the lattice parameter of the fcc structure. This formula can be applied to each peak and an average lattice parameter is calculated.

The determination of the lattice parameters of the hexagonal phase is more complicated. There exist two lattice parameters: c defining the vertical dimension and a defining the hexagonal base (considered to be equilateral). The parameter c can be determined from the position of the *hcp* (002) peak, while the position of the *hcp* (100) and *hcp* (110) peaks can be used in order to determine the parameter a.

It has to be noted that the precision of the lattice parameter calculation is limited, due to the low

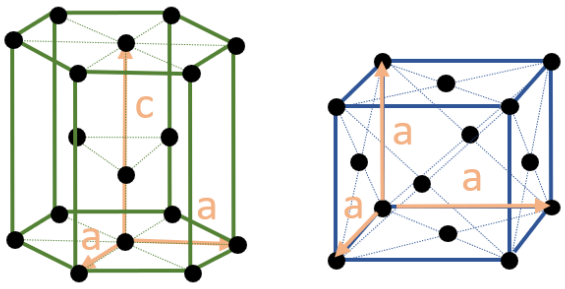

hcp *fcc*

signal intensity and the overlapping of *fcc/hcp* peaks. As a result, the exact peak positions cannot be determined very precisely.

Table S2. Lattice parameters estimates from the XRD diffraction peaks for the different samples analyzed in this work.

		200 nm with additives		200 nm no additives	
Angle 2θ (°)	Diffraction planes	*fcc* lattice parameter (Å)	*hcp* lattice parameter (Å)	*fcc* lattice parameter (Å)	*hcp* lattice parameter (Å)
41.6	*hcp* (100)	/	/	/	a = 2.5
44.3	*hcp* (002)/ *fcc* (111)	a = 3.55	c = 4.1	a = 3.55	c = 4.1
51.5	*fcc* (200)	a = 3.58	/	/	/
75.9	*hcp* (110)/ *fcc* (220)	a = 3.56	a = 2.5	a = 3.56	a = 2.5
92.4	*hcp* (112)/ *fcc* (311)	a = 3.55	/	a = 3.55	/
		Average: $a = 3.56$		Average: $a = 3.55$	

Supplementary characterization of the 50 nm sample with additives

The following X-ray diffraction (XRD) pattern comes from the analysis of Co nanowires grown in the 50 nm pores of a PC membrane, in presence of organic additives in the electrolyte. The precise synthesis conditions, as well as more details about the XRD experiments are presented in the main paper. As highlighted in the graph, the only four peaks that can be distinguished (44.5°, 64.5°, 77.5°, 81.9°) correspond to signal from the gold (Au) electrode attached to the bottom of the membrane, probably covering peaks corresponding to signal from *fcc*/*hcp* cobalt. No determination of the Co crystalline phase was therefore possible.

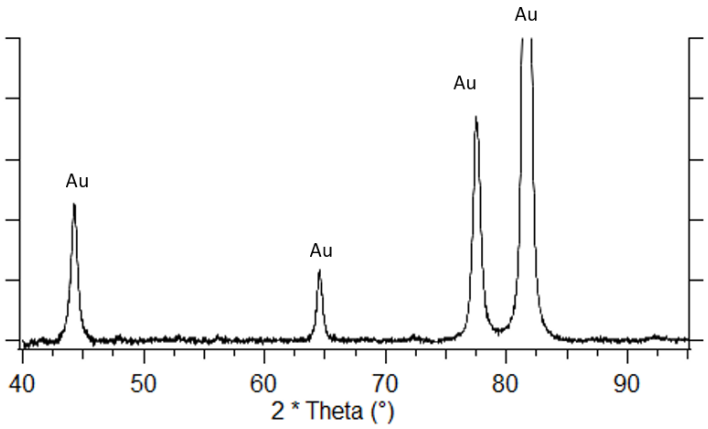

Figure S1. XRD pattern collected on 50 nm Co nanowires grown in the pores of a PC membrane in presence of organic additives in the electrolyte. The samples are analyzed with the membrane plane being in the XRD diffraction plane (*i.e.* the wire axis normal to the diffraction plane).

Supplementary characterization of the 50 nm without additives

The following results were obtained from wires grown into the 50 nm pores of a PC membrane, in absence of organic additives in the electrolyte. The characteristics of the membrane were the same as of the one used for the production of 50 nm nanowires deposited in presence of organic additives and are described in the main article. The composition of the electrolyte was the same as the one of the 200 nm nanowires without additives, namely: 240 g/L $CoSO_4 \cdot 7H_2O$ + 50 g/L $CoCl_2 \cdot 6H_2O$ + 40 g/L H_3BO_3.

XRD. The XRD pattern of this sample is shown in Figure S2.

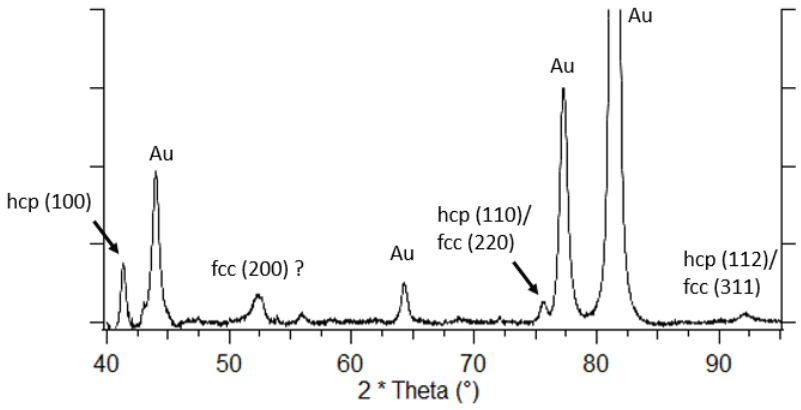

Figure S2. a XRD pattern collected on 50 nm Co nanowires grown in the pores of a PC membrane in absence of organic additives in the electrolyte. The samples are analyzed with the membrane plane being in the XRD diffraction plane.

Besides the 4 peaks corresponding to signal form the Au electrode still attached to the membrane, 3 peaks assigned to cobalt clearly can be distinguished: 41.5° (*hcp* (100), 75.9° (*hcp*

(110)/ *fcc* (220)) and 92.3° (*hcp* (112)/ *fcc* (311)). The two peaks around 52.5° and 56.0° cannot be assigned to neither Co, nor Au structures, even though the former one is close to the characteristic peak of *fcc* Co (200) around 51.5°. Due to the strong Au signal around 44.5°, peaks corresponding to *hcp* (002)/ *fcc* (111) cobalt might be covered, which makes it difficult to analyze the crystalline structure by XRD. Nevertheless, the relatively strong *hcp* (100) Co peak indicates that a significant part of the sample had a hexagonal crystalline structure with its *c*-axis perpendicular to the wire axis.

Magnetic hysteresis measurement. The magnetic properties of the 50 nm Co nanowires deposited in absence of organic additives were studied at room temperature with a magnetic field applied perpendicularly (⊥) or parallel (||) to the wire axis, as shown in **Figure S3**.

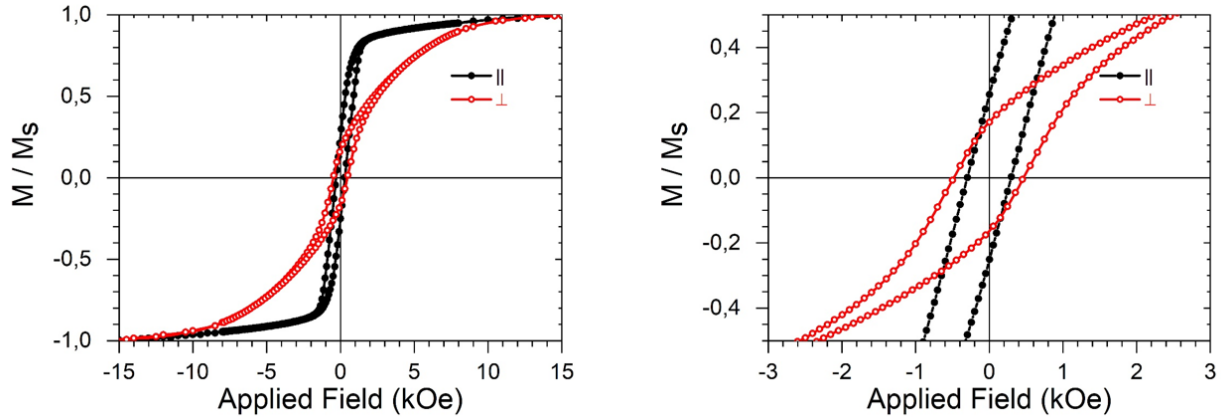

Figure S3. Magnetic hysteresis loops recorded on 50 nm Co nanowires grown in the pores of a PC membrane in absence of organic additives. The measurements were performed at ambient temperature with the field applied perpendicular (⊥, red hollow symbols) or parallel (||, black full symbols) to the cobalt wires. Left: full loops. Right: Zoom-in view of the full loops.

The loops are fairly similar to the ones observed on 50 nm Co nanowires deposited in presence of organic additives, shown in **Figure 4** a). Squared hysteresis loops with a coercivity of about

500 Oe measured on-axis (i.e. parallel) can be seen, as well as a clear magnetic easy axis parallel to the nanowires.

In Figure S4, the internal field (IF) NMR analysis in the frequency range associated with ^{59}Co resonances obtained from 50 nm nanowires without additives is represented. The spectrum (left) is mainly composed of two peaks, corresponding to cobalt in *fcc* multi-domain and *hcp* structures. In addition, a small peak around 216 MHz can be distinguished, which could be assigned to *fcc* stacking faults or *fcc* structures with a residual demagnetization field. The amount of *hcp* Co detected by NMR was significantly bigger than the amount of *fcc*, which differentiated this samples from all the other ones analyzed, where both phases were present in more or less the same quantity (**Figure S5**). The narrow peak width and the absence of a significant signal below 210 MHz (especially compared to the samples grown in presence of additives) suggest that cobalt was well crystallized, with big crystalline domains and few grain boundaries/ impurities. As the signal around 213 MHz can unambiguously be assigned to signal from fcc multi-domain structures and the optimal power is pretty much flat over the whole frequency range, it can be concluded that a major part of the signal arose from multi-domain structures and therefore the excitation of domain walls. The power needed for an optimal excitation and consequently also the enhancement factor is anisotropic, with less power needed for a parallel orientation between the *rf* field and the wire axis. This was the result a multi-domain structure and an easy axis of magnetization colinear with the wire, as confirmed by the magnetic hysteresis measurements (**Figure S3**). It could be concluded that the strong shape anisotropy of the 50 nm wires results was dominant over the *hcp* Co crystalline anisotropy (dipolar interactions could be neglected due to the big interwire distance), in contrast to the 200 nm sample synthesized under the same conditions. The NMR results showed the presence of a big amount of *hcp* Co in the sample but

gave no information about the orientation of its *c*-axis (easy axis of magnetization). The XRD analysis with the membrane plane in the diffraction plane, shown in Figure S2, suggested that a significant part of the sample had a hexagonal crystalline structure with its *c*-axis perpendicular to the wire axis. However, the presence of the gold electrode at the bottom of the membrane made it difficult to obtain more information by XRD.

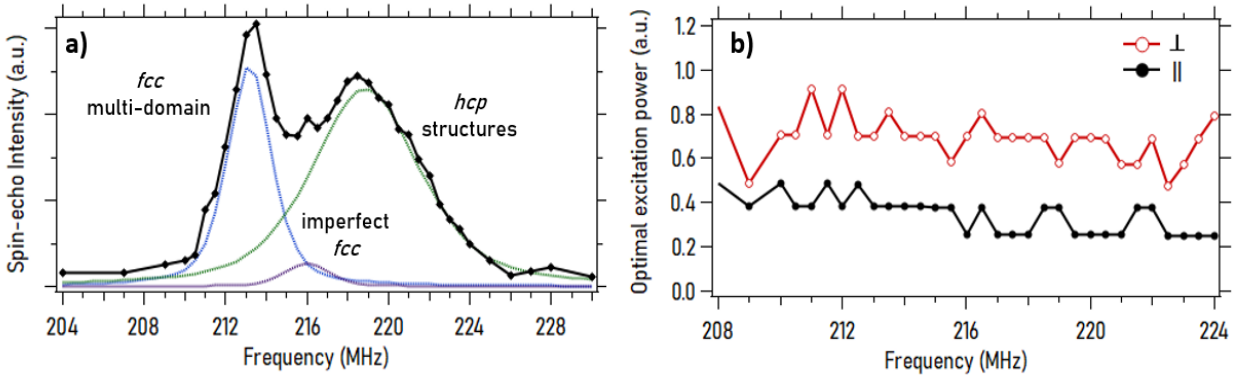

Figure S4. a) ^{59}Co IF NMR room temperature spectrum of 50 nm Co nanowires grown in PC membrane in absence of organic additives in the electrolyte. A tentative decomposition into peaks corresponding to different crystalline and magnetic structures is also presented, with the relative amounts of the different phases given in **Figure S5**. The spectral shape is identical regardless of the orientation between the *rf* pulse and the wire axis, so only one orientation is represented here. The graphs b) corresponds to the optimal excitation power for the same sample for different orientations: The red line (hollow spheres) corresponds to a perpendicular (⊥) orientation between the direction of the *rf* pulse and the wire axis, the black line (full spheres) to a parallel (||) one.

Overview of the measured relaxation times

The T_2 (spin-spin) relaxation time has been measured at three frequencies (213.5 MHz, 215.5 MHz and 218 MHz) for all the samples. The measured values for the different spectra represented in Figure 5 and Figure S4 are represented in Table S3. It can be seen that the T_2 relaxation time for the *fcc* Co multi-domain peak (213.5 MHz) is about 20-21 µs, while it is about 24-25 µs for the *hcp* Co peak (218 MHz). The value measured at 215.5 MHz (assigned to imperfect *fcc* Co) is generally in between those values. For a constant intensity of the *fcc* Co multi-domain peak, this leads to an about 5-15 % lower signal intensity after T_2 correction of the two other peaks.

In the literature, the T_2 values of different Co crystalline structures are not distinguished (it is generally given to be around 20-25 µs)[2]. As a result, it is difficult to use the T_2 data to assign help with the decomposition of the spectrum. Nevertheless, it was observed that the T_2 relaxation time is systematically the shortest for the *fcc* Co multi-domain phase, compared to the other ones.

Table S3. T_2 relaxation times measured for the different samples analyzed in this work.

	Additifs		No Additifs	
Frequency (MHz)	50 nm	200 nm	200 nm	50 nm
213.5	21 µs	21 µs	20 µs	21 µs
215.5	22 µs	23 µs	25 µs	25 µs
218	24 µs	24 µs	24 µs	25 µs

The T_1 (spin-lattice) relaxation time has also been measured for some samples using an saturation-recovery pulse sequence and values between 325 µs and 500 µs have been obtained,

which is in accordance with results obtained in the literature.[3] This justifies the short repetition rate (67 Hz) and shows that corrections of the spectrum intensity for this relaxation time are unsignificant.

Overview of the relative signal intensity of the different phases for the analyzed samples

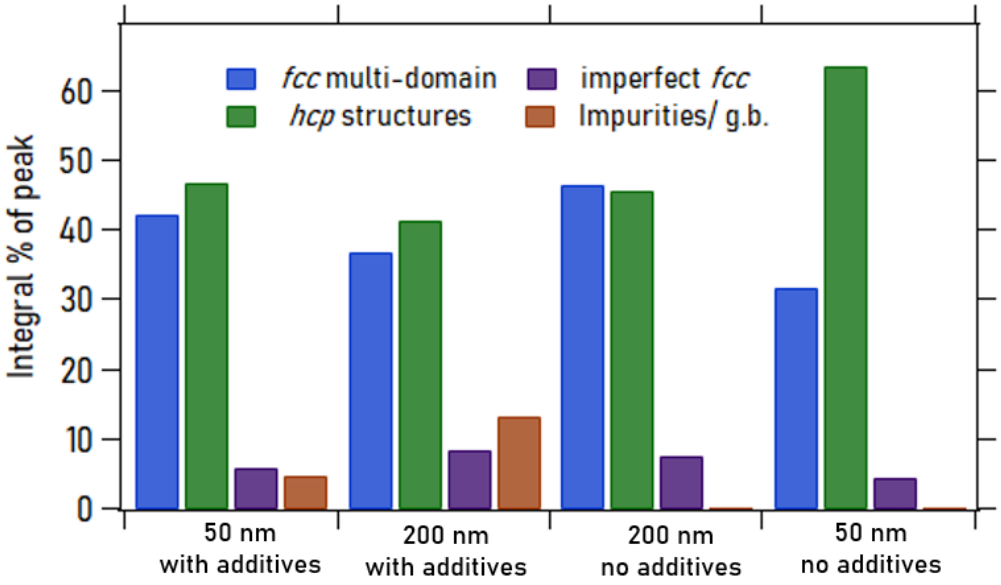

Figure S5. Quantitative distribution of the different crystalline/ magnetic phases detected by ^{59}Co IF NMR for the samples presented in this work. The corresponding spectra are shown in Figure 5 and Figure S4.

Fitting overview

The fitting of all the spectra has been performed using the DMFIT program and the detailed fitting parameters can be found in Table S4. For the samples synthesized in absence of additives in the electrolyte, the spectra can be fitted well with three peaks. In addition, only the position and width of the smallest peak were fixed in order to obtain the best fit.

For the samples synthesized in presence of additives in the electrolyte an additional peak needs to be added in order to account for grain-boundaries and impurities. Due to this additional peak,

the number of degrees of freedom had to be reduced in order to obtain a stable fitting (only the exact position of the 213 MHz peak and the intensity of all peaks were allowed to vary). However, the different peak positions and widths have been optimized manually.

Table S4. Fit parameters for the peaks of the decomposition of the ^{59}Co IF NMR spectra obtained from the different samples analyzed in this work. The star (*) behind a parameter signifies that this parameter was allowed to vary during the fitting procedure. The Gaussian/Lorentzian rate of the peak line shape was set to 0.5 for all peaks.

	Position (MHz)	Width (MHz)	Rel. Intensity (%)
50 nm PC additives	213.3*	3.0	42*
	218.5	5.6	47*
	215.5	2.5	6*
	210.0	3.5	5*
200 nm AAO additives	213.2*	3.0	37*
	218.5	5.6	41*
	216.0	2.5	9*
	210.0	3.5	13*
200 nm AAO no additives	213.3*	2.4*	47*
	218.9*	5.7*	46*
	216.0	2.5	8*
50 nm PC no additives	213.3*	2.4*	32*
	219.0*	6.1*	64*
	216.0	2.5	5*

References

(1) Holder, C. F.; Schaak, R. E. Tutorial on Powder X-Ray Diffraction for Characterizing Nanoscale Materials. *ACS Nano* **2019**, *13* (7), 7359–7365. https://doi.org/10.1021/acsnano.9b05157.

(2) Scarani, V.; Doudin, B.; Ansermet, J.-P. The Microstructure of Electrodeposited Cobalt-Based Nanowires and Its Effect on Their Magnetic and Transport Properties. *J. Magn. Magn. Mater.* **1999**, *205* (2–3), 8. https://doi.org/10.1016/S0304-8853(99)00513-2.

(3) Portis, A. M.; Gossard, A. C. Nuclear Resonance in Ferromagnetic Cobalt. *J. Appl. Phys.* **1960**, *31* (5), S205–S213. https://doi.org/10.1063/1.1984666.